Liquid meniscus condensation in dip-pen nanolithography

Joonkyung Jang, George C. Schatz, and Mark A. Ratner

Citation: The Journal of Chemical Physics **116**, 3875 (2002);
View online: https://doi.org/10.1063/1.1446429
View Table of Contents: http://aip.scitation.org/toc/jcp/116/9
Published by the American Institute of Physics

Liquid meniscus condensation in dip-pen nanolithography

Joonkyung Jang, George C. Schatz, and Mark A. Ratner
Department of Chemistry, Materials Research Center and Center for Nanofabrication and Molecular Self-Assembly, Northwestern University, Evanston, Illinois 60208

(Received 24 September 2001; accepted 5 December 2001)

The condensation of a liquid meniscus between a curved tip and a completely wetting substrate is theoretically studied in the context of dip-pen nanolithography (DPN). Utilizing the grand canonical Monte Carlo simulation of a two-dimensional lattice gas model, we studied the onset and broadening of menisci by tips with a range of curvatures. The tip–liquid interaction is characterized in terms of the wettability of the tip, and both wetting and drying tips are considered to mimic the various (hydrophilic and hydrophobic) ink molecule–water interactions possible in DPN. We study the microscopic details of the meniscus formation and examine the thermodynamic stability of the meniscus by focusing on the fluctuation in its width. After its initial formation, a meniscus grows continuously with increasing saturation (relative humidity), but the meniscus is typically wider than 10 molecular diameters until the saturation is sufficiently high that the entire interfacial region frills with liquid. For large tip–substrate distances, meniscus formation only occurs in the high saturation limit where conventional capillary condensation occurs. A general trend is that a sharp (small radius of curvature), dry tip results in a smaller meniscus width which further shrinks upon shortening the tip–substrate distance and/or raising temperature. At very short tip–substrate distances, the nascent meniscus is unstable and its width is independent of the tip curvature and wettability. The minimum width corresponds to a physical dimension of about 2.5 nm. © *2002 American Institute of Physics.* [DOI: 10.1063/1.1446429]

I. INTRODUCTION

When gases are confined to narrow (nano or microscale) pores or capillaries, their properties are significantly different from those of the bulk phase, and unique phase equilibrium properties emerge. Probably the most well known phenomenon is capillary condensation[1] in which a liquid uniformly fills a pore at a pressure (or chemical potential) *lower* than the bulk saturation pressure. At pressures still lower than the capillary condensation pressure, a discrete increase in the liquid layer on the solid (layering) or a sudden formation of a thick liquid film (prewetting) can occur. Most theoretical studies of capillary condensation so far have relied on idealized geometries such as infinitely long slits[2–7] and cylindrical pores.[8,9] Any real material however has a roughness that leads to geometrical and/or energetic heterogeneity on the solid surfaces. For such heterogeneous fluid–solid interactions,[10–14] it is found that an initial liquid condensation might occur preferentially in the regions where a solid wall attracts fluid strongly or fluid molecules are geometrically more confined. With increasing pressure, this liquid bridge[11] or meniscus formed between solid surfaces undergoes further capillary condensation to a liquid state in which the entire pore is filled with liquid.

The onset of a liquid meniscus between solid surfaces has important implications for the recently discovered phenomenon of dip-pen nanolithography (DPN).[15,16] In typical DPN experiments (Fig. 1), a sharp (radius curvature <20 nm) atomic force microscope (AFM) tip coated with ink molecules is brought to the substrate surface in ambient conditions. Then water molecules in the air condense between the tip and substrate, triggering a downward flow of ink molecules (designed to form a self-assembled monolayer on the substrate) from the tip (see Fig. 1). With this novel technology, it is now possible to construct molecular patterns on solids with nanoscale resolution. Direct observation of the water meniscus has not been made, and the ultimate resolution, exact mechanism, and thermodynamic dependence of DPN are not known. We believe the resolution of DPN depends crucially on the existence and width of the water meniscus between the tip and substrate. In this paper, we present a theoretical investigation of the microscopics of liquid meniscus formation relevant to DPN experiments.

There are numerous theoretical approaches to condensation in confined geometries, the most common of which include the macroscopic Kelvin equation,[7,17,18] mean-field density functional theory (DFT),[3–5,10,11,13,19] Monte Carlo (MC) simulation,[2,6,9,14,20,21] and molecular dynamics (MD) simulation.[7,8] Although all of these theories could be used to describe DPN, there are important limitations to most. Macroscopic theories are questionable for describing systems whose dimensions are only several molecular diameters,[22] which is likely the typical tip–substrate distance in DPN. In addition, any macroscopic theory is not expected to give us insight into the microscopic details of condensation (e.g., fluctuation in the meniscus, an exact density profile of the meniscus, etc.). DFT probably has played a leading role in predicting phase behavior over a whole range of thermodynamic states. It provides qualitatively (in many cases, quantitatively) correct results for average density profiles, but it is limited in its ability to define stability information such as arises with fluctuations in the meniscus width. To follow

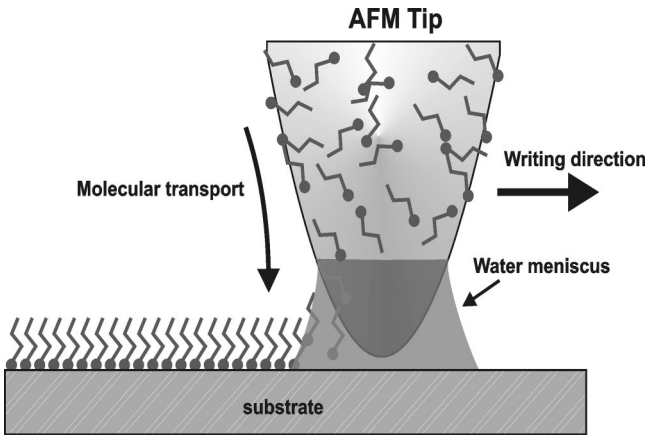

FIG. 1. A diagram illustrating the suggested mechanism of the DPN experiment. As an AFM tip coated with ink molecules is brought close to a substrate (typically gold) surface, water in the air condenses between the tip and substrate. The ink molecules, designed to form a self-assembled monolayer on the substrate, are then transferred through the meniscus to the substrate. By moving the tip parallel to the substrate surface, one can write patterns with nanoscale resolution.

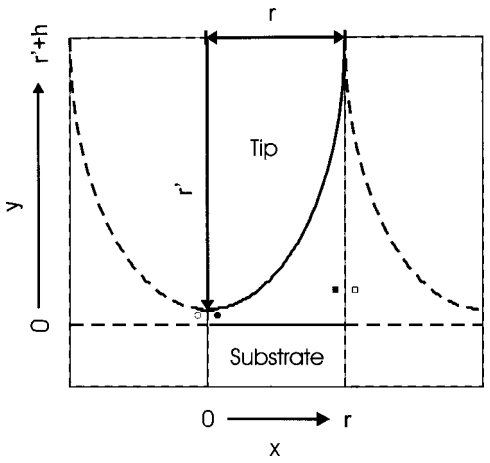

FIG. 2. The geometry of our system and the adopted boundary condition. A two-dimensional plane is represented by a discrete square lattice, and our system is confined vertically (in y direction) between the substrate surface located at $y=0$ and an elliptic tip surface with horizontal and vertical axes with lengths r and r', respectively. The tip is separated from the substrate by h lattice spacings. The horizontal range of the system is between $x=0$ and $x=r$ in units of lattice points, and corresponds to the right half of the elliptic tip. The tip surface drawn in the figure refers to the aspect ratio, $r'/r=2$, and looks a little corrugated because the surface is defined as a collection of lattice sites closest to the continuous elliptic line. The boundary condition at the horizontal ends of our system is reflecting: a site at $x=-1$ (open circle in the figure) is taken to be the mirror image of a site at $x=1$ (filled circle) with respect to the $x=0$ line. Likewise, a site at $x=r+1$ (open square) is the mirror image (with respect to $x=r$) of a site at $x=r-1$ (filled square).

such fluctuations, we need to examine our system at thermodynamic equilibrium on a configuration by configuration basis. To do this we have chosen the grand canonical Monte Carlo (GCMC) simulation as our method, which is convenient for investigation of phase equilibria. MD simulations would be another choice, but these are not likely to be practical for systems of the size we are interested in.

Instead of realistically simulating water menisci in a specific DPN experiment (e.g., an AFM tip coated with octadecanethiol on a gold surface[15,16]), we opt to examine qualitative behavior of the meniscus for a range of geometric and energetic parameters within a simple model. Specifically, the water is modeled as a two-dimensional lattice gas confined between a flat substrate surface and a tip that is modeled as an ellipse. We systematically vary the tip curvature and its distance from the substrate as well as the fluid–tip and fluid–substrate interaction strengths. A useful measure of the fluid–solid attraction strength that is commonly utilized in the experimental characterization of organic films on solid surfaces[23,24] is the wettability of the solid surface by the liquid.[25,26] By measuring the contact angle between the solid–gas and liquid–gas interfaces, solid surfaces can be categorized into completely (contact angle$=0°$) and partially ($0°<$contact angle$<180°$) wetting or even drying (contact angle$=180°$) surfaces, in decreasing order of fluid–solid attraction.[27]

We take the fluid–substrate interaction in our study to be a typical H_2O–metal binding energy,[28] so that the substrate is completely wet at all temperatures.[29] The tip surface coated with ink molecules, however, can be hydrophilic or hydrophobic depending both on the tip itself and on the ink molecule coating that tip. Usually, an AFM tip in DPN is coated with large alkane thiols (octadecanethiol, for example), which is quite hydrophobic. In this case, the tip can be modeled as a partially wetting or drying tip using the terminology described above. However in some experiments, the alkane thiols have been functionalized with amine or carboxylic acid groups, which would tend to make the tips more hydrophilic. In addition, some experiments have been done with oligonucleotide inks that should be quite hydrophilic. In view of this, we consider a range of tip properties, including completely and partially wetting and partially drying tips.

This paper is organized as follows: In Sec. II, we describe in detail our lattice gas model, the system geometry, and the method used in the GCMC simulation. We also explain how we choose the wettability of the tip and the temperature relevant to the water meniscus in modeling typical DPN experiments. Results from simulations are reported in Sec. III. The microscopic details of the meniscus are discussed in Sec. III A with an emphasis on the average density profile and fluctuations in the meniscus width for each configuration generated in the simulations. The dependence of the meniscus width on tip curvature, wettability, and distance of the tip from the substrate are systematically studied in Sec. III B. Section IV summarizes our conclusions.

II. SIMULATION DETAILS

A. Lattice gas model on a square lattice

The fluid is modeled as a two-dimensional lattice gas on a square lattice bounded by an elliptic tip surface and a flat substrate surface (as shown in Fig. 2). In this model, each lattice site is either empty or occupied by just one particle, and each occupied site interacts with its (occupied) nearest neighbor sites with an attractive energy ϵ. Particles are confined vertically between the lower flat substrate surface located at $y=0$, and the upper elliptic tip surface (see Fig. 2)

separated from each other by h lattice spacings. The ellipse has axis lengths of r and r' lattice spacings in the horizontal (x) and vertical directions, respectively, and the elliptic surface is defined as the collection of lattice points nearest to the continuous elliptic line. In the horizontal direction, our system ranges from $x=0$ to $x=r$, thus only simulating the right half of the elliptic tip. A reflecting boundary condition is invoked at the horizontal ends of the system: a particle at $x=-1$ (the open circle in the Fig. 2) taken to be the mirror image of the particle at $x=1$ (the filled circle in the figure) with respect to the $x=0$ line. Similarly, a particle at $x=r+1$ (the open square in the figure) is the mirror image of the one at $x=r-1$ (the filled square in the figure) with respect to the vertical line at $x=r$. These reflecting boundary conditions, which are compatible with symmetry of the system at equilibrium are invoked in an effort to simulate a (two times) bigger system in the horizontal direction with the same amount of computational time. The lattice sites in our model are naturally divided into bulk, tip surface, and substrate surface sites. A site positioned at (x,y) is taken to be a tip surface site if its upper nearest neighbor site, $(x, y+1)$, belongs to the tip surface. A tip surface site feels an attractive binding energy b_T as well as the nearest neighbor attraction ϵ. The sites directly above the substrate surface ($y=0$) are defined as the substrate surface sites and are attracted to the substrate with a binding energy b_S, as well as to their nearest neighbors with an energy ϵ. All the rest are bulk sites for which only the nearest neighbor attraction ϵ is allowed. As a result, the Hamiltonian of our model can be written as

$$H=-\epsilon \sum_{\substack{\text{nearest}\\ i,j=\text{neighbor pair}}} c_i c_j - b_S \sum_{i=\substack{\text{substrate}\\ \text{surface}}} c_i - b_T \sum_{i=\substack{\text{tip}\\ \text{surface}}} c_i , \tag{2.1}$$

where c_i is the occupation number (0 or 1) for the ith site.

The lattice gas system described above is designed to mimic the region between the end of the tip and the substrate in a DPN experiment. With the reasonable assumption that our system is in thermal and phase equilibrium with a bulk reservoir specified by temperature T and chemical potential μ, we perform a GCMC simulation. The relevant Hamiltonian for GCMC is $H-\mu N$ (N=number of occupied sites). It is well known that a lattice gas model in a grand canonical (μVT) ensemble is equivalent to an Ising model in a canonical (NVT) ensemble.[30] We thus adopt standard single spin flip dynamics for Ising magnets with Metropolis importance sampling[31] and interpret the results utilizing the correspondence $c_i \leftrightarrow (1-S_i)/2$, where S_i is the spin value (1 or -1) of the ith site. For a given total number of sites of the system, N_{tot}, one MC step is defined as attempting a single spin flip move N_{tot} times. For each spin flip move, the position of the spin to flip is determined by randomly selecting (separately) the x and y positions of the site to flip. Since the tip surface has a curvature (see Fig. 2), this means that sites around the vertical end of the tip (near $x=0$ where the sites are geometrically more confined in the vertical direction) are sampled more often (typically 2 or 3 times more often) than the other sites. For most of runs, the initial configuration of the lattice is chosen to be bulk-gaslike and the corresponding gas branch behavior is studied as the chemical potential is raised toward the bulk gas–liquid transition. Specifically, for the gas branch we take the initial lattice sites to be occupied randomly to give an average occupation of 1/4 occupied lattice. Liquid branch behavior is also studied by choosing the initial lattice randomly occupied to give an average occupation of 3/4. Typically, we start with 40 000 MC steps for equilibration, and then 10 000 lattice configurations (sampled every 12 MC steps) out of 120 000 configurations are generated for evaluating the average occupancy of each lattice site and determining the liquid meniscus width for each configuration.

We calculated the density profile, $\rho(x,y)$, which is defined as the average occupancy of the site located at (x,y). Then the meniscus width is determined from the density profile, $\rho(x,y)$ as follows. Noting that average site occupancies for bulk liquid and gas are always above and below 1/2, respectively, each site in our system is called a *liquid site* if its average occupancy is above 1/2, and a *gas site* if it is less than 1/2 full on average. For each horizontal position x, we checked vertically the average occupancies of sites of the column ranging from the lower substrate surface to the upper tip surface. If all the sites of a column are more than half full on average [$\rho(x,y)>1/2$ for all y], it is declared to be a *liquid column*. Then the *meniscus width* is defined as a relative width of liquid columns,

$$\text{Meniscus width} = [2\times(\text{number of liquid columns})-1]/(2r+1), \tag{2.2}$$

where the number of columns ranges from 1 to $r+1$, and the factor of 2 is to take into account the left half of our tip surface (Fig. 2). The meniscus width is declared zero if no liquid column exists. According to this definition, the (relative) meniscus width ranges from zero (when no column exists) to one (when the entire lattice is liquidlike). Note also that our meniscus width defined this way refers to the waist width of a concave liquid meniscus.

We also followed the instantaneous meniscus width for each configuration generated in the simulation. The same definition as in Eq. (2.2) applies to the meniscus width, but the liquid column in this case is defined differently. For each configuration, the occupancy of each site is either zero (empty) or one (occupied), so a liquid column is now defined as a column fully occupied by particles from the substrate to tip surface. We calculated the average meniscus width based on the width for each configuration and found no difference (within the fluctuation in the width, see below) from the width from density profile.

To address the issue of meniscus stability, we calculated for every GCMC run the *fluctuation* defined as

$$\text{Fluctuation} = \sqrt{\langle(\text{Meniscus width}^2\rangle - \langle\text{Meniscus width}\rangle^2}, \tag{2.3}$$

which is the standard deviation in the configuration-dependent meniscus width. The meniscus width for each configuration in Eq. (2.3) is similarly defined as in Eq. (2.2) and is the (configuration-dependent) width relative to the

horizontal range of our system, $2r+1$. Then the *instability* is defined as the fluctuation, Eq. (2.3), relative to the average meniscus width,

$$\text{Instability} = \text{Fluctuation}/\langle \text{Meniscus width} \rangle. \tag{2.4}$$

The sharpness of tip is characterized in terms of aspect ratio, α, defined as

$$\alpha = r'/r. \tag{2.5}$$

The radius of curvature at the vertical end of the tip is then given by r/α. We take $r=70$ for our calculation, meaning our system size for a circular tip ($r=r'$) typically ranges from 1300 (for $h=4$) to 3810 (for $h=24$) sites. To see the finite size effect of our simulation box, we also examined bigger simulation boxes by increasing the horizontal radius by a factor of 2 ($r=140$) and 3 ($r=210$) for a tip–surface distance $h=8$. In doing so, we need to increase the aspect ratio correspondingly (by 2 or 3 times) to keep the geometry (radius of curvature) around the vertical end of tip invariant. We then compared the meniscus widths for $\alpha=1$ and $r=70$, $\alpha=2$ and $r=140$, and $\alpha=3$ and $r=210$ (all of which have a radius of curvature of 70 lattice spacings). Within the fluctuations in meniscus width (typically 10%), the average meniscus widths for several thermodynamic state are found to be invariant to the size of simulation box.

B. Temperature and geometric and energetic parameters relevant to DPN

Considering the simplicity of our model described above, it seems difficult to identify the geometric and energetic parameters which will realistically resemble the water meniscus in a specific DPN experiment. However, in order to derive maximum physical insight from these calculations, we will give rough but reasonable estimates of some of the geometric and energetic parameters. With these parameters, we will later (in Sec. III) attempt to connect our results to DPN experiments.

Temperature is reported in terms of a reduced temperature defined as $T^*=T/T_c$, where T_c is the bulk critical temperature for the lattice gas model. This is known exactly to be $k_BT_c/\epsilon=(1/2)/\ln(1+\sqrt{2})$.[30] In the GCMC simulations, we study a range of temperatures, $0.4 \leqslant T^* \leqslant 0.6$, which covers normal temperatures of DPN experiments (the freezing and boiling temperatures of water are $T^*=0.42$ and $T^*=0.58$, respectively). Most of results are presented for water at room temperature, $T^*=0.46$. In the lattice gas model, Eq. (2.1), the chemical potential, μ_c, at which the bulk gas–liquid transition occurs is also known exactly as $\mu_c=-2\epsilon$ (temperature independent). For a given temperature T, simulations are run by varying the saturation defined as

$$\text{Saturation} = \exp[(\mu-\mu_c)/k_BT]. \tag{2.6}$$

The saturation defined above is in the ideal gas limit the pressure relative to the bulk saturation pressure for the gas–liquid transition. This, of course, is just the definition of relative humidity. In studying meniscus condensation, the saturation was continuously increased from zero to one. The saturation at which a liquid column condenses is located up to a resolution of $\mu/\epsilon=0.005$.

In our lattice model, the nearest neighbor distance in the liquid phase is one lattice spacing. Referring to the TIPS model,[32] the typical nearest H_2O–H_2O distance in water could be approximated as the Lennard-Jones diameter for the O–O interaction, 3.24 Å. Then, the horizontal radius of the tip chosen in this study, $r=70$, is estimated to be $r\sim 23$ nm, which is a typical radius of curvature (<20 nm) of the tip used in DPN. The tip–substrate distance is a variable in DPN experiments. It is expected to be several molecular diameters when the tip is in near contact with the substrate. We take the shortest tip–substrate distance to be one lattice spacing ($\sim$6.4 Å) and vary the distance up to 24 lattice spacings ($\sim$78 Å). To study the effect of tip curvature on DPN resolution, we systematically vary the aspect ratio, $\alpha=r'/r$, of the elliptic tip as $\alpha=0.5, 1, 2, 3$ with r fixed to 70 lattice spacings (23 nm). Then the corresponding radius of curvature (r/α) at the end of the tip is 46 nm, 23 nm, 12 nm, and 8 nm, respectively.

We now attempt to set energetic parameters in our simulation. Since we are interested in the density profile and width of the meniscus, only the relative magnitudes of surface binding energies with respect to the fluid–fluid interaction, b_T/ϵ and b_S/ϵ, are important. The binding energy to the substrate surface is chosen to emulate water on gold surface which is the most common substrate in DPN.[15,16] The hydrogen bond strength of water molecules is typically 15–25 kJ/mol and H_2O usually binds to metals with strengths of 40–65 kJ/mol.[28] Based on the above numbers, the attraction to the substrate surface is three times stronger (compared to fluid–fluid interaction), so we have taken $b_S/\epsilon=3$ throughout. For our flat substrate surface in a square lattice model, the wetting behavior is known exactly in terms of the magnitude of the fluid–solid binding energy relative to the fluid–fluid attraction, b_S/ϵ.[33] The fluid–substrate interaction chosen above gives rise to a complete wetting of the substrate by the liquid as the gas pressure approaches bulk saturation.[33] In our two-dimensional system, the *contact angle* is defined as the angle between the solid-gas interface line and the solid–liquid interface line at the contact point of the solid (the substrate in this case), liquid, and gas, and complete wetting means the angle is zero (see the Introduction).

The tip surface–water interaction is less well known because the tip is coated with various ink molecules (octadecanethiol, 16-mercaptohexadecanoic acid, for example). As discussed in the Introduction, depending on the ink molecules, the tip surface could be either hydrophilic or hydrophobic. To model this situation, we consider three types of tip surface interactions that differ in their wettabilities. Unlike the flat substrate surface described above, the wetting behavior of the curved tip surface is not known, and we refer to a flat solid surface whose wetting behavior (in a square lattice gas model) is exactly known in terms of b_T/ϵ.[33] The tip wettability described below corresponds to that of the flat tip surface. We first have chosen a strongly attracting tip with a binding energy of $b_T/\epsilon=3$ (the same attraction as the substrate) so that it is completely wetting (CW) at all temperatures. For weakly attracting tips, we have selected tips with $b_t/\epsilon=3/4$, and $b_T/\epsilon=1.4$. In the temperature range consid-

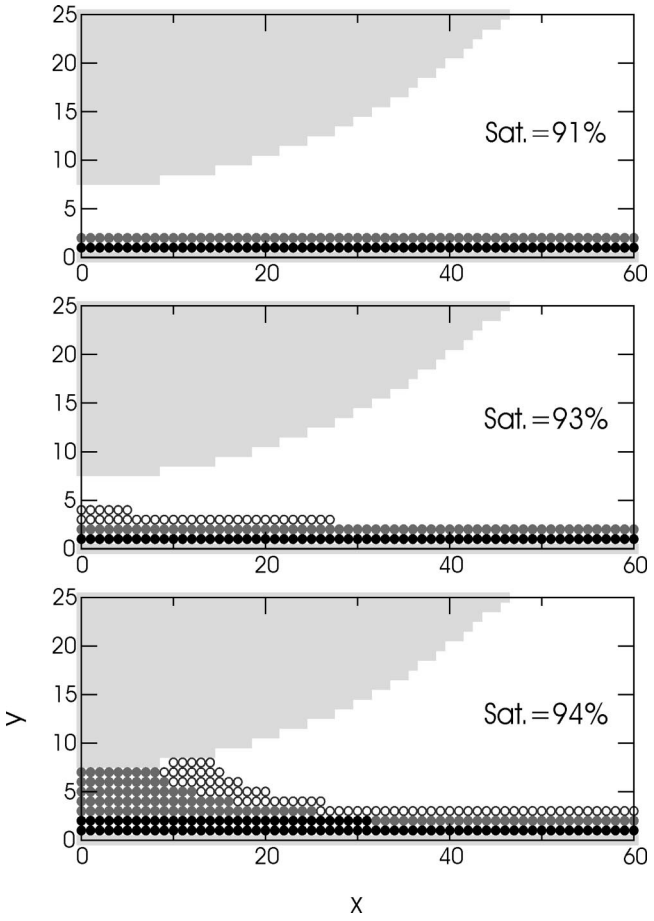

FIG. 3. Variation in liquid meniscus formation with increasing saturation (with the temperature fixed at $T^*=0.46$) for a partially drying tip with circular ($\alpha=1$) shape. The tip–substrate distance is fixed at $h=8$ lattice spacings. The lattice points with a dense gas density ($\rho=0.25-0.5$) are drawn as open circles, and the grey and black filled circles represent liquid densities with $\rho=0.5-0.75$ and $\rho=0.75-1$, respectively. Initially, the system is gaslike except near the substrate which is covered with liquid layers (top). As the saturation increases, dense gas condenses around the end of the tip at 93% saturation (middle), and finally leads to a liquid meniscus at 94% saturation (bottom).

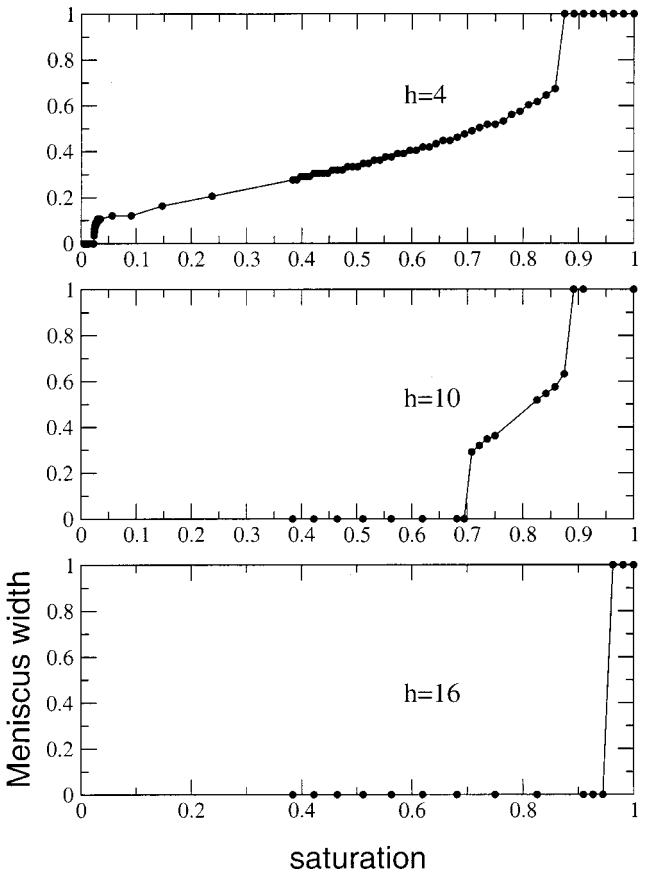

FIG. 4. Isotherms ($T^*=0.46$) of meniscus formation and broadening at several tip–substrate distances for a completely wetting circular tip. For short tip–substrate distances ($h=4$ and $h=10$), two consecutive transitions occur. The first jump in the width defined in Eq. (2.2) corresponds to the onset of a liquid meniscus and the second to filling of the entire system with liquid. In between, there is a continuous broadening of the meniscus. At the largest distance ($h=16$) however, the two transitions collapse into a single gas–liquid transition which is characteristic of the conventional capillary condensation.

ered ($0.4<T^*<0.6$), the tip with $b_T/\epsilon=3/4$ is always partially wetting (PW) since the tip is completely wet only at temperatures above the wetting temperature, $T^*=0.863$.[33] The tip with the weakest attraction, $b_T/\epsilon=1/4$, is called partially drying (PD) because, at temperatures above a drying temperature ($T^*=0.863$), the tip is completely dry.[33,34] But the tip is only partially drying at all the temperatures studied here. The binding energy of PD tip is chosen close to the value of $b_T/\epsilon\sim 20\%$ suggested by Luzar and Leung[35] in their lattice gas modeling of a hydrophobic surface.

III. RESULTS

A. Mechanism of meniscus formation

We first show how the equilibrium density profile changes from a gaslike state to a liquid meniscus as the saturation increases at constant temperature and tip–substrate distance. In Fig. 3, density profiles (at a temperature $T^*=0.46$) for 3 saturations, 91% (top), 93% (middle), and 94% (top), are drawn for the partially drying circular ($\alpha=1$) tip separated from the substrate by 8 lattice spacings. In the figure, open circles represent dense gas sites defined as sites with average occupancy between 1/4 and 1/2. Gray and black circles correspond to liquid sites with densities between 1/2 and 3/4 and between 3/4 and 1, respectively. Before the meniscus formation, the completely wetting substrate is already covered with two layers of liquid, but the tip is dry (top and middle). As the saturation reaches 93% (middle), dense gas forms around the tip end, and a liquid meniscus results if the saturation is further increased to 94% (bottom). The accumulation of dense vapor preceding liquid meniscus formation is in accord with observations made in simulating capillary condensation in nanoslits.[20] Note that the liquid–gas interface in the meniscus is diffuse, indicating the instability of the initial meniscus which we will describe later.

Once initially formed, does the meniscus broaden continuously until it fills the entire system as saturation further increases? In Fig. 4 are drawn isotherms ($T^*=0.46$) of the meniscus width defined in Eq. (2.2) for a completely wetting circular tip that is separated from the substrate by 4 (top), 10 (middle), and 16 (bottom) lattice spacings. For the two

shorter tip–substrate distances, one can clearly see that the meniscus broadens continuously after its initial formation until it shows another jump in width which corresponds to an abrupt filling of the region outside of the meniscus. This is similar to the splitting of the gas–liquid capillary condensation into a gas–liquid bridge transition and a liquid bridge–liquid transition, as observed in density functional studies of energetically heterogeneous slitlike pores.[31] As the tip–substrate distance increases, the initial (minimum) meniscus width increases and the range of saturations in which the continuous filling occurs decreases (middle). At the longest tip–substrate distance shown (bottom), the two transitions collapse into a conventional capillary condensation in which the entire system gets uniformly filled with liquid. This conventional capillary condensation is of little relevance to DPN, so we focus our attention on the initial formation and continuous broadening of the meniscus. The broad range of the continuous filling found for the shortest tip–substrate distance has an important implication for possible thermodynamic control of DPN. Based on our rough estimate of the physical dimension of the lattice (Sec. II B), the result shows that, at a tip–substrate distance of 1.3 nm, the width of meniscus can be continuously tuned from 4.5 nm to 32 nm by controlling the pressure (or humidity).

We also checked meniscus evaporation for the same geometries in Fig. 4 by studying the liquid branch behavior (running simulations starting from initially liquidlike configuration, see Sec. II A). Except for the first transition (meniscus formation) for $h=4$, the resulting meniscus evaporation curves, together with the condensation curves in Fig. 4, form hysteresis loops characteristic of a first order phase transition. The rounded jump in the meniscus width and absence of hysteresis loop imply that the first transition for $h=4$ is supercritical due to the small system size. For other transitions in the figure, the saturations at which true thermodynamic transitions occur are expected to be lower than those in the figure. The exact location of true thermodynamic transition may be found using a thermodynamic integration technique, for example.[2] In view of qualitative nature of this work, we do not attempt to find the exact transition points but rather focus on the gas branch behavior hereafter.

Figure 5 illustrates the density profile change as the tip approaches the substrate at constant temperature and pressure ($T^*=0.46$ and 70% saturation) for a completely wetting circular tip. The symbols are drawn in the same way as described in Fig. 3. At the longest tip–substrate distance ($h=11$) (top), the system is gaslike, whereas the tip and substrate are covered by liquid layers. As the tip–substrate distance decreases by one lattice spacing (middle), a meniscus forms, but the liquid–gas interface is rather diffuse at this point. This again indicates that the initially formed meniscus is rather unstable, but it should be noted that this meniscus is also of minimal width and this is preferred for increasing the resolution of DPN. Unlike the case where saturation is increased for fixed geometry and temperature (Fig. 3), we do not see an accumulating dense gas before formation of the meniscus. As the tip gets even closer to the substrate ($h=9$) (bottom), the meniscus broadens and is stabilized in the sense that the liquid–gas interface is sharper.

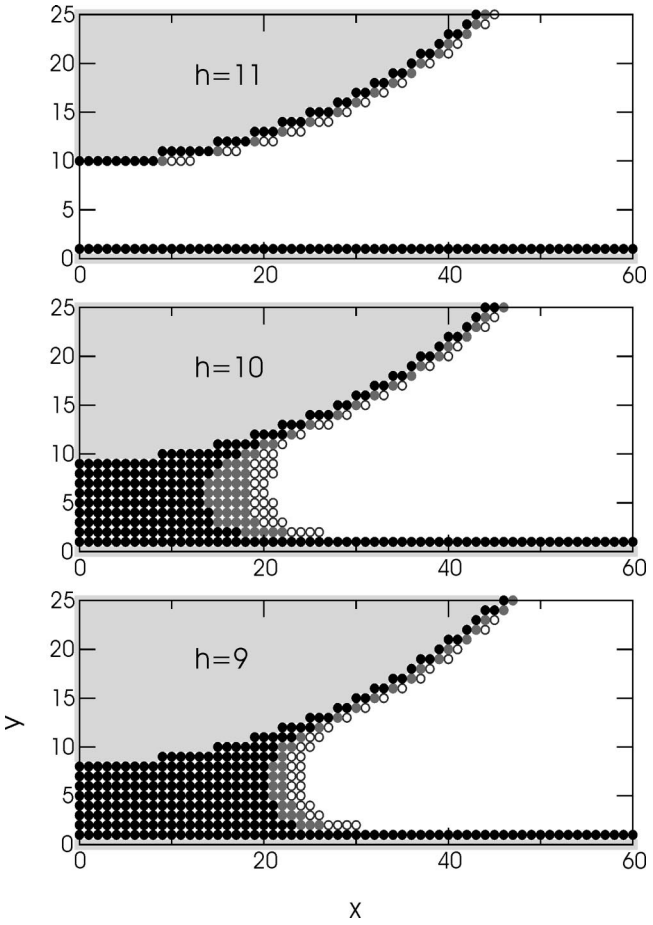

FIG. 5. Picture of the liquid meniscus as the tip approaches the substrate at constant temperature ($T^*=0.46$) and saturation (70%). As in Fig. 3, the sites with dense gas density ($\rho=0.25-0.5$) are drawn as open circles, and the gray and black filled circles represent liquid densities with $\rho=0.5-0.75$ and $\rho=0.75-1$, respectively. The tip is completely wetting and circular in shape ($\alpha=1$). Both the tip and substrate surfaces are covered with layers of liquid for large tip separations where there is no meniscus (top). As the tip–substrate distance reaches 10 lattice spacings ($h=10$), a liquid meniscus forms and its boundary is rather fuzzy (middle). Further decreasing the tip–substrate distance results in broadening of the meniscus and thinning (and thus stabilizing the meniscus) of the gas–liquid interface (bottom).

How different are the individual (equilibrium) configurations from the average density profile? Figure 6 illustrates three individual configurations that were taken from the simulations with a partially wetting circular tip under a thermodynamic condition of 90% saturation and $T^*=0.46$. Each circle in these snapshots represents an occupied site. The shape of meniscus fluctuates significantly from configuration to configuration. Out of 10 000 such configurations, the average occupancy of each site is calculated, and liquid sites with average occupancy above half are drawn in the lower left. The average and standard deviation of the meniscus width in this case are about 51 and 6 lattice spacings, respectively, meaning that the relative fluctuation is more than 10%. It is this fluctuation that leads to the diffuseness of the liquid–gas interface (Figs. 3 and 5) and which destabilizes the meniscus.

To further pursue the issue of meniscus stability, we checked the fluctuation in the meniscus width for various tips

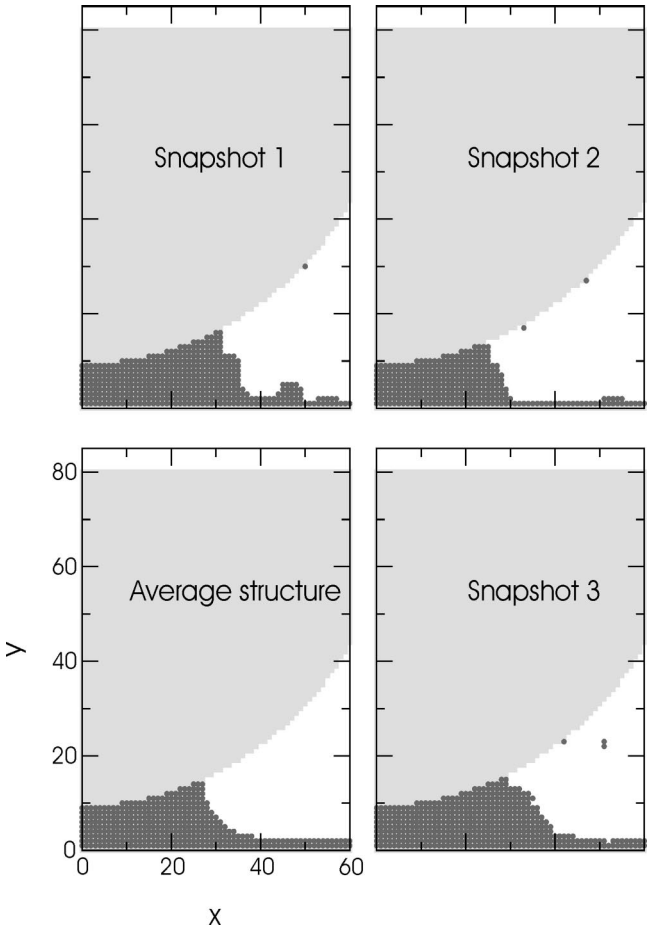

FIG. 6. Individual equilibrium liquid configurations and average structure generated from a Monte Carlo simulation for a partially wetting circular tip at temperature $T^*=0.46$ and 90% saturation. In the three figures starting from the upper left clockwise, drawn as circles are the occupied lattice sites, illustrating fluctuations in the liquid configurations. In the lower left, circles represent sites whose average density is liquidlike (more than half occupancy on average). 10 000 snapshots are sampled from 120 000 equilibrium configurations generated in the simulation. The meniscus width from the average liquid structure (lower left) is 55 lattice spacings (note only the right half of the tip is shown in the figure). The average and fluctuation, Eq. (2.3), for the configuration dependent width of the meniscus are 51 and 6 lattice spacings, respectively.

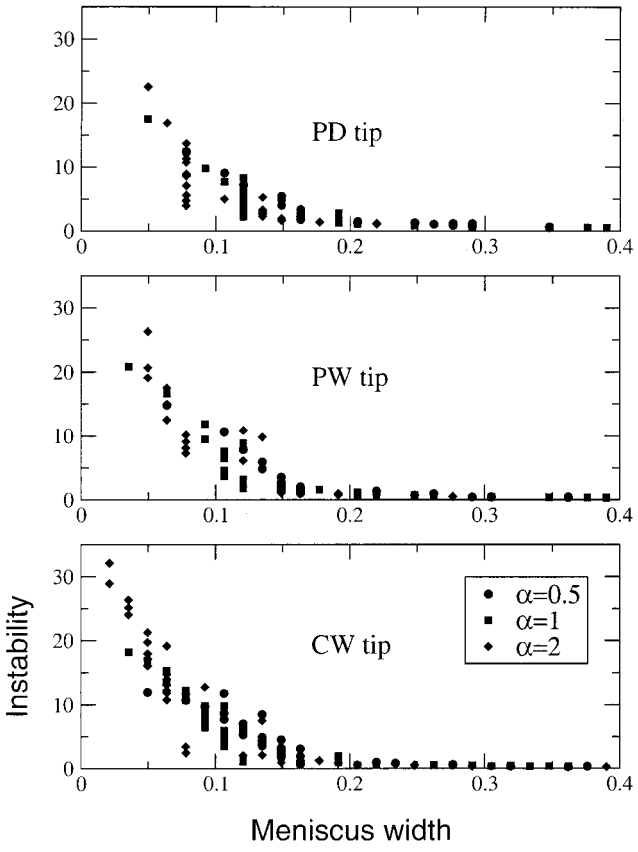

FIG. 7. Instability of the meniscus vs its width. At a fixed temperature, $T^*=0.46$, the saturation, Eq. (2.6), is increased, leading to formation and broadening of the meniscus until the entire system is filled with liquid. Among the multitude of menisci, only meniscus widths up to 0.4 are shown in the figure. The fluctuation, Eq. (2.3), and average of the meniscus width were calculated for various tip–surface distances (ranging from 4 to 24 lattice spacings). The plot shows the instability defined in Eq. (2.4) as a function of the average meniscus width for partially drying (top), partially wetting (middle), and completely wetting (bottom) tips. For each tip, its curvature is also varied as $\alpha=0.5$, 1.2. In the figure, the multiple points for a given width refers to the instabilities for different tip–substrate distances. Huge instabilities for small menisci (with width less than 0.1) are noticeable, and the menisci get stabilized as they broaden. No appreciable dependence on the tip curvature is found.

with different wettability, curvature, and distance from the substrate. For every combination of parameters above, we followed meniscus formation along an isotherm ($T^*=0.46$) by increasing the saturation, Eq. (2.6), up to 100%. For each case specified by its thermodynamic state and geometric and energetic parameters, the meniscus widths for 10 000 configurations (out of 120 000 configurations) generated in the simulation have been collected, and the instability defined in Eq. (2.4) is calculated. In Fig. 7, we plot the instability of meniscus as a function of its average width. Data are plotted for partially drying (top), partially wetting (middle), and completely wetting (bottom) tips. For each tip, the curvature and distance from the substrate are varied as $\alpha=0.5$, 1, 2 and $h=4-24$ (with an interval of 4) lattice spacings, respectively. In the figure, multiple values of the instability for a given meniscus width and tip curvature represent different tip–surface distances. Although data are scattered, we can clearly see that the instability decreases with broadening of the meniscus and converges (typically, to 0.2) at widths above 0.3. Also note that small menisci with relative width less than 0.1 are very unstable, the fluctuations being far larger than their averages. Small menisci for the partially drying tip look less unstable than other tips, but considering their large instabilities the difference seems immaterial. We also find from the figure that the curvature of tip plays no role in determining the meniscus stability.

B. Dependence on the geometry and energetics

We now explore the effects of relative geometry of the tip with respect to the substrate and its wettability. In Fig. 8, we illustrate how the changing the tip curvature effects the meniscus for a completely wetting tip by fixing the thermodynamic condition ($T^*=0.46$, 50% saturation). Liquid sites with density above 50% are shown as circles for the tip aspect ratios, $\alpha=0.5$, 1, 2, 3. The completely wetting tip and substrate give rise to contact angles near zero: that is, the

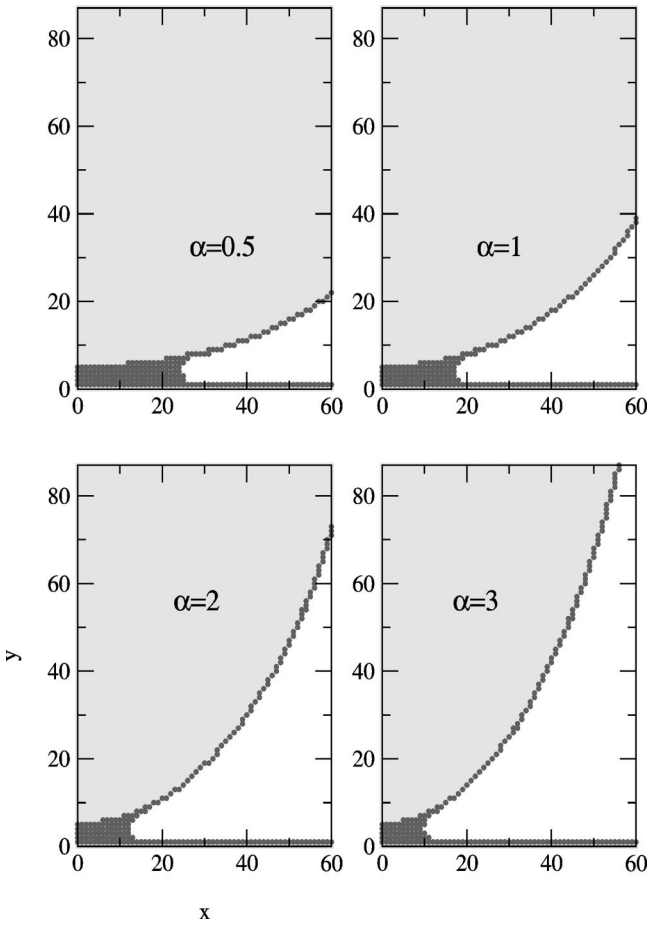

FIG. 8. Tip curvature dependence of the meniscus at constant temperature ($T^*=0.46$) and saturation (50%). As the aspect ratio of the elliptic tip, α, increases from 0.5 to 3, the meniscus width decreases to half its original size. Drawn as circles in the figures are lattice sites with a liquid density (above half occupancy on average). The tip is a completely wetting tip.

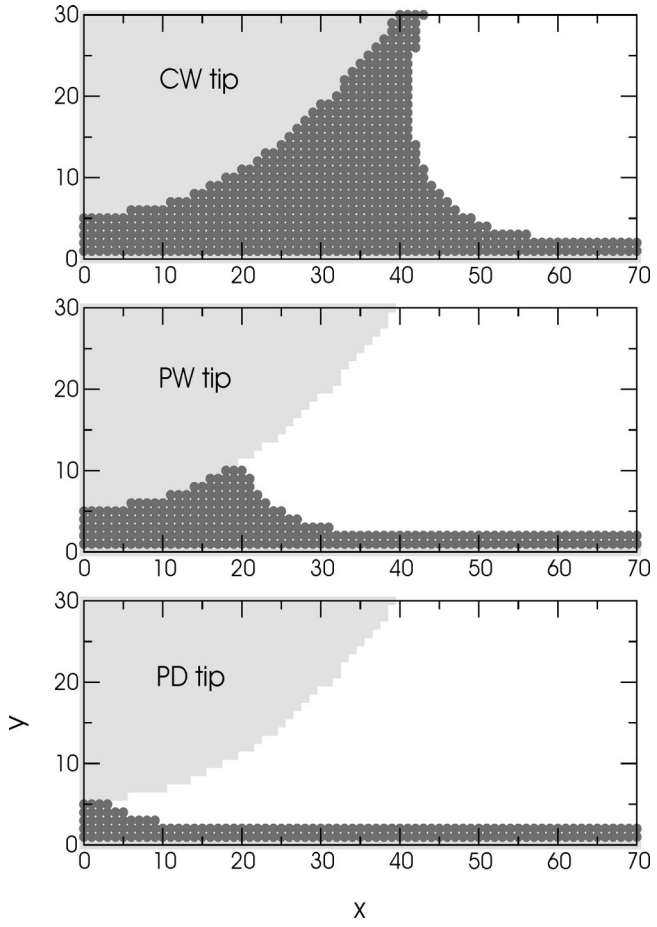

FIG. 9. Dependence of the meniscus on the tip wettability for fixed temperature and saturation ($T^*=0.46$ and 91% saturation). The binding energy of an elliptic tip (with a curvature of $\alpha=2$) is varied from completely wetting (top), partially wetting (middle), to partially drying (bottom). From the density profile calculated from the GCMC simulations, lattice points with liquid densities (more than half occupied) are drawn as circles. As the tip gets drier (its wettability changes from completely wetting to partially wetting and drying) the meniscus width reduces dramatically.

liquid–gas interface is parallel to the substrate, and tangential to the elliptic tip surface. As the tip gets sharper, we notice an appreciable decrease in the meniscus width from 48 ($\alpha=0.5$) to 18 ($\alpha=3$) lattice spacings (note only the right half of tip is shown in the figure). This dramatic change in the width with the curvature tells us that tip sharpness is crucial in achieving higher resolution in DPN experiments.

How does the meniscus depend on the wettability of the tip for a given thermodynamic condition? At 90% saturation, we changed the wettability of the tip (separated from the substrate by 6 lattice spacings) from completely wetting (top), partially wetting (middle), to partially drying (bottom) (Fig. 9). Evidently, changing wettability has an even more dramatic effect than the tip curvature effect shown in Fig. 8. Here the meniscus gets smaller in width by a factor of 10 as the wettability reduces from complete wetting to partially drying. We also note that the contact angle (the angle between the tip–gas interface line and the liquid–gas interface line at the contact point of the tip, liquid, and gas) for the partially wetting tip is about 90°, and the angle is nearly 150° for the partially drying tip. The above findings suggest that increasing the dryness of the ink molecules (making the molecule more hydrophobic) will enhance the resolution of DPN.

Probably the most convenient variable in a DPN experiment is the tip–substrate distance. To determine how this changes the meniscus width, we varied the tip–substrate distance starting from 1 lattice spacing (the closest distance possible in our lattice model) under 70% saturation. The results for circular tips with different wettabilities are shown in Fig. 10 at several temperatures, $T^*=0.4$ (top), 0.46 (middle), 0.52 (bottom). The meniscus width from the density profile, Eq. (2.2), is plotted, along with the fluctuation in width, Eq. (2.3), drawn as error bars. In general, we see a linear decrease in width with increasing the tip–substrate distance. For the completely wetting ($T^*=0.4, 0.46$) tip and the partially wetting ($T^*=0.4$) tip at low temperatures however, there is a sudden decrease of the width to zero at a critical distance, which can be interpreted as a ''snap-off'' of the liquid meniscus. The meniscus width for the partially drying tip and the wetting tips at higher temperatures smoothly go to zero. The maximum distance for which a meniscus is allowed decreases as the tip gets drier. As in Fig. 9, we observe that a drying tip results in narrower menisci than wetting tips for all the temperatures considered, $T^*=0.4$, 0.46, 0.52.

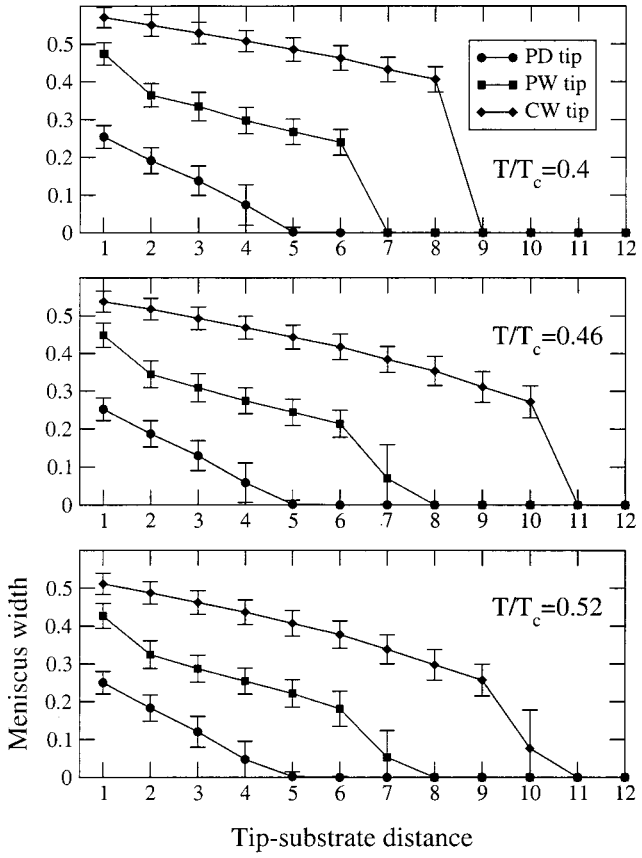

FIG. 10. Tip–substrate distance dependence of the meniscus width. For a circular ($\alpha=1$) tip, the tip–substrate distance is varied from 1 to 12 lattice spacings at several temperatures, $T^*=0.4$ (top), 0.46 (middle), 0.52 (bottom), by fixing the saturation at 70%. The partially drying tip shows a linear decrease in width down to zero with increasing tip separation from the substrate. For a partially ($T^*=0.4$) or completely wetting ($T^*=0.4, 0.46$) tip at low temperatures however, the width decrease linearly with increasing the separation up to a finite value, and then falls abruptly to zero (a "snap off" of the meniscus). For each width in the figure, the fluctuation in width, Eq. (2.3), is also shown as an error bar.

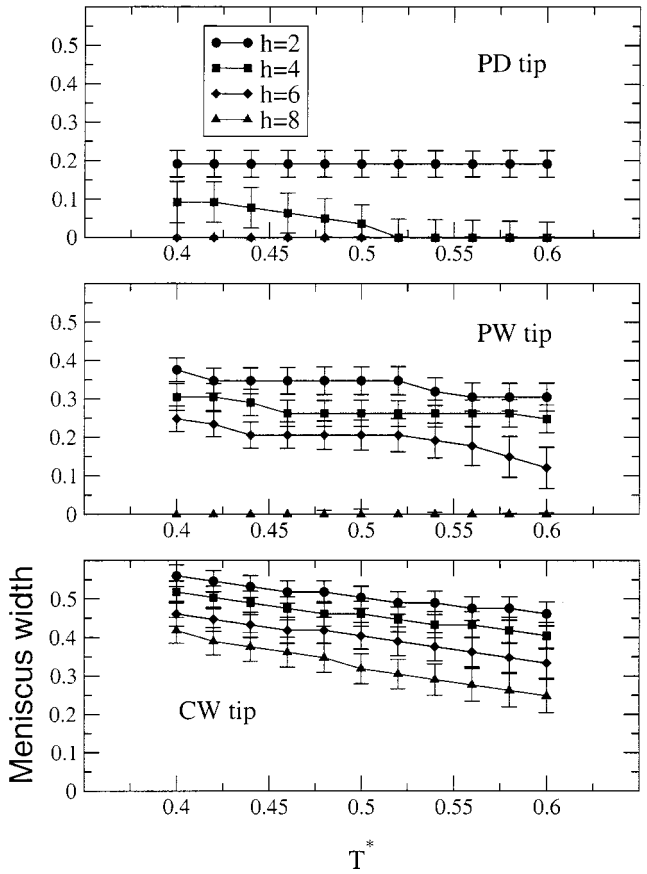

FIG. 11. Temperature dependence of the meniscus width for a circular tip at a constant (70%) saturation. For short tip–surface distances (=2,4,5,8 lattice spacings, the meniscus width, Eq. (2.2), is studied by varying temperature in the range $0.4\leqslant T^*\leqslant 0.6$. In general, the liquid meniscus evaporates with increasing temperature, and thus its width decreases. The partially drying tip (top) closest (separated by 2 lattice spacings) to the substrate is however insensitive to temperature, and so is the partially wetting tip (middle) in the temperature range, $T^*=0.46-0.52$.

We now look more closely at the temperature dependence of the menisci considered in Fig. 10. Under the same saturation (70%), we study a range of temperatures, $0.4\leqslant T^*\leqslant 0.6$, covering the melting ($T^*=0.42$) and boiling ($T^*=0.58$) temperatures of water. In Fig. 11, the meniscus widths for some short tip–substrate distances ($h=2,4,6,8$ lattice spacings) are plotted by varying temperature. Here we see that the meniscus generally narrows with increasing temperature. The drying tip (top) closest ($h=2$) to the substrate however is completely insensitive to the temperature increase while for $h=4$ the meniscus width gets smaller for higher temperatures. For the partially wetting tip, we see plateaus in the width at temperatures ranging from 0.46 to 0.52. The meniscus widths for the completely wetting tip monotonically decrease with temperature. Although not shown in the figure, we find that there is an inversion in the temperature dependence of the width for certain tip–substrate distances. This can be seen in Fig. 10, for $h=9$ and 10 lattice spacings, where the menisci form (the widths change from zero to finite) with increasing temperature from $T^*=0.4$ (top) to $T^*=0.46$ (middle), but then they get smaller upon increasing the temperature to 0.52 (bottom). For all other tip–substrate distances, the meniscus narrows with temperature rise as observed in Fig. 11. Overall, in the range of temperatures studied, the temperature effect on the meniscus width is not as great as that which comes from varying the saturation (Figs. 3 and 4), the tip curvature (Fig. 8), its wettability (Fig. 9), or its separation from the substrate (Figs. 5 and 10).

At a given temperature, what is the minimum saturation (relative humidity in DPN) necessary for a meniscus to form? At temperature, $T^*=0.46$ (the temperature corresponding to water at room temperature, see Sec. II B), we located the minimum saturation for meniscus condensation for tips with various curvatures, wettabilities, and separations from the substrate (ranging from 4 to 24 lattice spacings). Figure 12 shows resulting meniscus condensation lines as functions of saturation and the tip–substrate separation for tips with curvatures of $\alpha=0.5$ (top), 1 (middle), and 2 (bottom). For each tip curvature, the wettability of the tip is varied from partially drying to partially and completely wetting. The lines in the figure are just to connect data points obtained from the simulation. A meniscus forms when a gas-like state (a point in the plane left of the condensation line) crosses the line toward a lower tip–substrate distance and/or

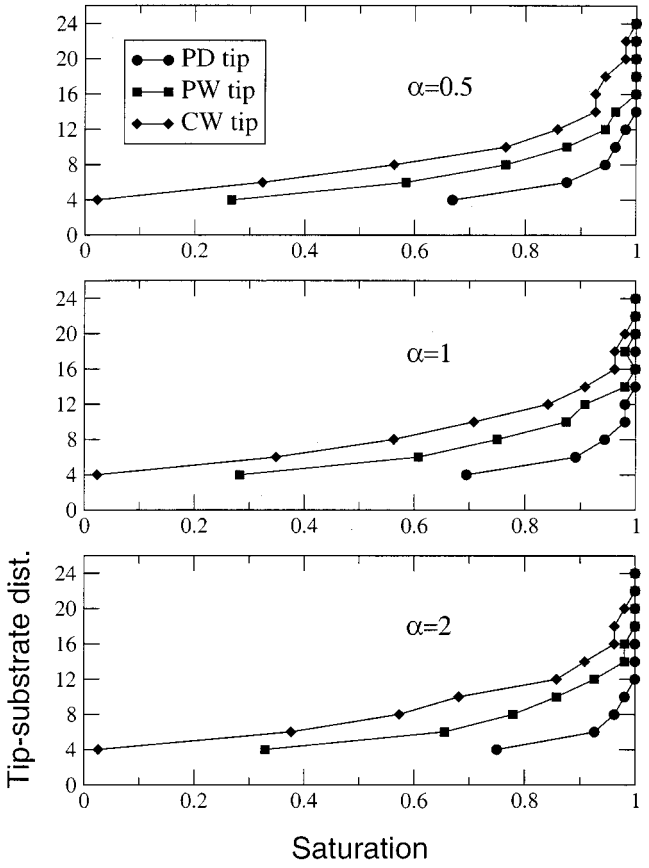

FIG. 12. Isothermal meniscus condensation line as a function of saturation and tip–substrate distance. A meniscus forms as saturation approaches the line from left and/or tip–substrate distance decreases from above the line at a constant temperature, $T^*=0.46$. Decreasing the tip–substrate distance results in dramatic shifts of the condensation points toward lower saturation. Only the uniform filling of the system with liquid is allowed at large tip–surface separation, and the line approaches the bulk gas–liquid condensation line (saturation=1). Increasing the tip wettability shifts the meniscus condensation line toward lower saturation. Decreasing the tip curvature also causes menisci to form at lower saturation, but the effect is minor.

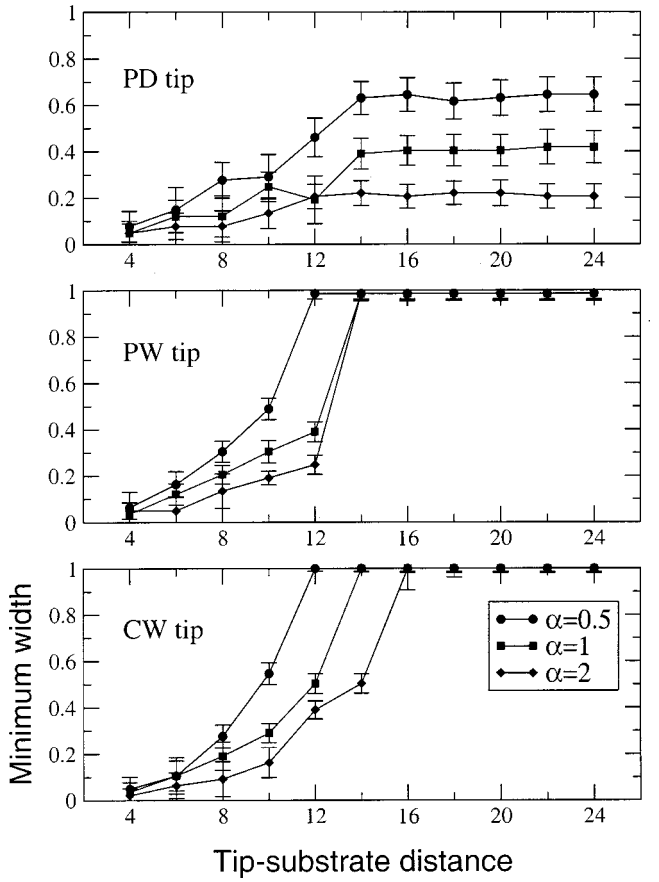

FIG. 13. Minimum meniscus width vs tip–substrate distance at a constant temperature ($T^*=0.46$). For a given tip–substrate distance, the onset of a meniscus has been located by increasing the saturation from zero. The width of the nascent meniscus, which is the minimum width, is studied for tips with various wettabilities and curvatures ($\alpha=0.5,1,2$). As the tip–substrate separation increases, the minimum width for a partially drying tip (top) converges to a value less than one (a finite meniscus), which decreases with increasing the tip curvature. For a partially (middle) or completely (bottom) wetting tip however, only the entire filling of the system with liquid (meniscus width =1) is allowed at large tip–substrate separations. At shorter separations, the minimum width generally decreases with increasing tip curvature. At the shortest approach of the tip to the substrate (four lattice spacings) however, the minimum width converges to a value independent of tip curvature and wettability.

a higher saturation. The second transition line discussed for the isotherms in Fig. 4 is not drawn since our interest here is in the onset of meniscus formation. Qualitatively, all the lines have the same shape in that they are shifted significantly toward lower saturation with decreasing tip–substrate distance. For example, for a completely wetting tip at its closest approach to the substrate (4 lattice spacings), a meniscus begins to form at only 2% saturation. At large tip–substrate distances, the line approaches the bulk gas–liquid condensation line (vertical line at saturation=1), and, as found in Fig. 4, only uniform filling of the system with liquid is possible. The condensation lines show systematic shifts toward lower saturations with increasing the tip wettability. As the tip gets sharper (α increasing from 0.5 to 1 and 2), the lines are generally shifted toward higher saturations, but the tip curvature effect is not as pronounced as that of wettability.

We now try to answer the question, ''What is the minimum width of liquid meniscus possible under the thermodynamic conditions relevant to DPN?''. This issue is germane to the ultimate resolution of DPN although we should note that additional processes (diffusion and deposition) are likely to be equally important. We have already learned that the answer depends on the tip curvature, its wettability, and its distance from the substrate. The condensation lines drawn in Fig. 12 only give us the saturation at which the initial (thus minimal in width) meniscus forms. To answer this question, we use the same temperature ($T^*=0.46$), tip curvatures, $\alpha=0.5$, 1, 2, and the tip–substrate distances, $h=4,...,24$ as in Fig. 12, and we calculated the minimum width for each combination of parameters described above. The results are shown in Fig. 13 for partially drying (top), and partially (middle), and completely (bottom) wetting tips. Along with the width from density profile, Eq. (2.2), we show the fluctuation in width, Eq. (2.3), as error bars in the figure. We first note that the minimum width converges to a constant value for large tip–substrate distances (typically above $h=16$ lattice spacings). For the wetting tips, the constant value corre-

sponds to the system entirely filled with liquid, but for the drying tip it is a meniscus which gets smaller as the tip is sharpened. For intermediate tip–substrate distances, e.g., $h=8,10,12$ lattice spacings, we see that the minimum width decreases as the tip gets sharper. The minimum width however shows no pronounced dependence on the wettability of the tip, in contrast to the systematic dependence of the minimal saturation for meniscus formation on the wettability found in Fig. 12. The most striking observation is that, for the shortest tip–substrate distance, $h=4,6$ lattice spacings, the width is nearly independent of curvature and wettability, considering the fluctuation shown in the figure. We thus see another convergence in the width in the short tip–substrate distance limit. Due to the smallness in width and relatively large fluctuation, the menisci in the short tip–substrate distance limit are expected to be very unstable (for stability analysis, see Fig. 7). We conclude that a nascent meniscus formed by a tip at its closest approach to the substrate is independent of the tip geometry and wettability. When converted to a physical dimension relevant to DPN (see Sec. II B), the minimal meniscus width for the shortest distance in Fig. 13 is estimated (taking the minimum width for $h=4$ to be 0.05) to be 2.3 nm.

IV. SUMMARY AND CONCLUSION

Motivated by the notion that the formation of a water meniscus between the AFM tip and substrate is a crucial and triggering event in DPN, we presented a theoretical study of the liquid condensation that occurs in a confined geometry similar to that found in DPN. Given that the exact geometry of the tip and the nature of molecular interactions in DPN are not known, we have chosen to study a simple lattice gas model and to examine the qualitative behavior of the liquid meniscus by considering a variety of possible tip geometries and their distances from the substrate. The energetics of the tip–liquid interaction is characterized by the wettability of the tip surface, and both wetting and drying tips are studied, emulating hydrophilic and hydrophobic tips in DPN. The geometric and energetic parameters in our simulation have been related to typical DPN experiments in a rough but reasonable way.

Qualitatively, our study shows that the meniscus width is a sensitive thermodynamic variable which decreases dramatically with increasing tip curvature, separation from the substrate and/or with decreasing its wettability. The temperature dependence of the meniscus is only modest in the range relevant to typical DPN experiments. By closely following the density profile, we have been able to observe the mechanism of meniscus formation as the tip–surface distance decreases or the system is more saturated with water. Meniscus stability was also investigated by examining fluctuations in the individual configurations generated from the simulation.

Our simulations have demonstrated that the width of the meniscus can be continuously tuned over a broad range by changing the saturation (Fig. 4). This provides a convenient approach for controlling pattern resolution in DPN, but one should note that we have assumed in this analysis that DPN is under thermodynamic control, and further that pattern width is directly related to meniscus width. Regarding the ultimate resolution of DPN, the minimum width has been found to be on the order of 10 molecular diameters ($\sim$2 nm, see Sec. III B), but this meniscus at its minimal size is unstable due to large fluctuations compared to its size. Since an unstable meniscus is not expected to give reliable molecular transport from the tip in DPN, the ultimate resolution of DPN is likely to be larger than this (currently, 15 nm is the finest resolution in DPN[16]).

In addition to improving our model to simulate more realistically the thermodynamic equilibrium properties of the water meniscus in DPN, we are interested in two dynamic features of DPN: the transport of the ink molecules through the meniscus and their subsequent self-assembly to form a monolayer on the substrate. In a recent paper, we have begun to address these other features with the assumption of a constant flux of ink molecules to the substrate using an infinitely sharp tip, no meniscus, and a stochastic diffusion model to describe pattern formulation and self assembly.[36] It is our hope that we can combine the equilibrium aspects from the present work with this dynamics modeling to develop a more complete picture of DPN in the future.

ACKNOWLEDGMENTS

This research was supported by AFOSR MURI Grant No. F49620-00-1-0283. We thank Seunghun Hong and Chad Mirkin for helpful discussions and for providing Fig. 1. We are also grateful to Paul Sheehan for important discussions.

[1] For reviews of phase behavior in narrow pores, see R. Evans, J. Phys.: Condens. Matter **2**, 8989 (1990); L. Gelb, K. E. Gubbins, R. Radhakrishnan, and M. Sliwinska-Bartkowiak, Rep. Prog. Phys. **62**, 1573 (1999).
[2] K. Binder and D. P. Landau, J. Chem. Phys. **96**, 1444 (1992); E. V. Albano, K. Binder, and W. Paul, J. Phys. A **30**, 3285 (1997).
[3] E. Bruno, U. M. B. Marconi, and R. Evans, Physica A **141A**, 187 (1987); R. Evans, U. M. B. Marconi, and P. Tarazona, J. Chem. Phys. **84**, 2376 (1986).
[4] E. Cheng, M. R. Swift, and M. W. Cole, J. Chem. Phys. **99**, 4064 (1993).
[5] R. Evans and P. Tarazona, Phys. Rev. Lett. **52**, 557 (1984).
[6] B. K. Peterson and K. E. Gubbins, Mol. Phys. **62**, 215 (1987); C. L. McCallum, T. J. Bandosz, S. C. McGrother, E. A. Muller, and K. E. Gubbins, Langmuir **15**, 533 (1999).
[7] T. Yoshioka, M. Miyahara, and M. Okazaki, J. Chem. Eng. Jpn. **30**, 274 (1997); M. Miyahara, H. Kanda, T. Yoshioka, and M. Okazaki, Langmuir **16**, 4293 (2000).
[8] G. S. Heffelfinger, F. van Swol, and K. E. Gubbins, Mol. Phys. **61**, 1381 (1987); G. S. Heffelfinger, F. van Swol, and K. E. Gubbins, J. Chem. Phys. **89**, 5202 (1988).
[9] B. K. Peterson, K. E. Gubbins, G. S. Heffelfinger, U. Marini Bettolo Marconi, and F. van Swol, J. Chem. Phys. **88**, 6487 (1988); B. K. Peterson, G. S. Heffelfinger, K. E. Gubbins, and F. van Swol, *ibid.* **93**, 679 (1990).
[10] C. Chmiel, K. Karykowski, A. Patrykiejew, W. Rzysko, and S. Sokolowski, Mol. Phys. **81**, 691 (1994).
[11] P. Rocken and P. Tarazona, J. Chem. Phys. **105**, 2034 (1996); P. Rocken, A. Somoza, P. Tarazona, and G. Findenegg, *ibid.* **108**, 8689 (1998).
[12] Y. K. Tovbin and E. V. Votyakov, Langmuir **9**, 2652 (1993).
[13] H. Bock and M. Schoen, Phys. Rev. E **59**, 4122 (1999); M. Schoen and H. Bock, J. Phys.: Condens. Matter **12**, A333 (2000).
[14] W. Gac, A. Patrykiejew, and S. Sokolowski, Surf. Sci. **306**, 434 (1994); K. Karykowski, W. Rzysko, A. Patrykiejew, and S. Sokolowski, Thin Solid Films **249**, 236 (1994).
[15] R. D. Piner, J. Zhu, F. Xu, S. Hong, and C. A. Mirkin, Science **283**, 661 (1999).
[16] S. Hong and C. A. Mirkin, Science **288**, 1808 (2000); S. Hong, J. Zhu, and C. A. Mirkin, *ibid.* **286**, 523 (1999).
[17] R. Evans and U. M. B. Marconi, Chem. Phys. Lett. **114**, 415 (1985); R.

Evans and U. M. B. Marconi, J. Chem. Phys. **86**, 7138 (1987).
[18] L. R. Fisher and J. N. Israelachvili, J. Colloid Interface Sci. **80**, 528 (1981).
[19] U. M. B. Marconi and F. van Swol, Europhys. Lett. **8**, 531 (1989); Phys. Rev. A **39**, 4109 (1989).
[20] W. J. Stroud, J. E. Curry, and J. H. Cushman, Langmuir **17**, 688 (2001).
[21] A. Papadopoulou, F. van Swol, and U. Marini Bettolo Marconi, J. Chem. Phys. **97**, 6942 (1992).
[22] A grand canonical Monte Carlo simulation study of three dimensional lattice gas model for a slitlike geometry shows that Kelvin equation fails for surface distances less than 10 lattice spacings. See Ref. 2.
[23] J. P. Fokers, P. E. Laibinis, and G. W. Whitesides, Langmuir **8**, 1330 (1992); P. E. Laibinis, G. M. Whitesides, D. L. Allara, Y. Tao, A. N. Parikh, and R. G. Nuzzo, J. Am. Chem. Soc. **113**, 7152 (1991); G. M. Whitesides and P. E. Laibinis, Langmuir **6**, 87 (1990).
[24] S. D. Evans, R. Sharma, and A. Ulman, Langmuir **7**, 156 (1991).
[25] R. Pandit, M. Schick, and M. Wortis, Phys. Rev. B **26**, 5112 (1982).
[26] S. Dietrich, in *Phase Transition and Critical Phenomena*, edited by C. Domb and J. L. Lebowitz (Academic, New York, 1988), Vol. 12.
[27] Alternatively, complete wetting is often described as formation of a macroscopically thick liquid film on the solid as pressure is increased from the gas side toward the bulk gas–liquid transition pressure. Similarly, complete drying is defined as development of a macroscopic gas film on the solid as pressure is decreased from the liquid side toward the bulk gas–liquid coexistence pressure. It can be shown (Ref. 25) that the complete wetting (drying) defined this way leads to zero (180°) contact angle.
[28] P. A. Thiel and T. E. Madey, Surf. Sci. Rep. **7**, 221 (1987).
[29] Water adsorption on (polycrystalline) gold is known to exhibit monolayer coverage at 33% relative humidity at room temperature. See, S. Lee and R. W. Staehle, Mater. Trans., JIM **37**, 1768 (1996).
[30] T. L. Hill, *Statistical Mechanics* (McGraw–Hill, New York, 1956), Chap. 7.
[31] K. Binder and D. Stauffer, in *Application of the Monte Carlo Method in Statistical Physics*, 2nd edition, edited by K. Binder (Springer, Berlin, 1987).
[32] W. L. Jorgensen, J. Chem. Phys. **77**, 4156 (1982).
[33] Within a square lattice gas model, the wetting (drying) behavior of a flat solid surface (a line in two dimensions) is determined exactly by the fluid–surface attraction, b, relative to the fluid–fluid attraction, ϵ. For $b/\epsilon>1$, the surface is completely wettable at all temperatures. In case of a weakly attracting solid surface, $1/2<b/\epsilon<1$, completely wetting occurs only at temperatures above a wetting temperature, and for an even weaker attraction, $b/\epsilon<1/2$, the surface is completely dry at temperatures above a drying temperature. In both cases, the wetting or drying temperature is given by (Refs. 25, 34) $e^x[\cosh x-\cosh(x-2bx/\epsilon)]=\sinh x$, $x=\epsilon/2k_BT$. Note that wetting and drying temperatures are symmetric with respect to $b/\epsilon=1/2$.
[34] D. B. Abraham, Phys. Rev. Lett. **44**, 1165 (1980).
[35] A. Luzar and K. Leung, J. Chem. Phys. **113**, 5836 (2000).
[36] J. Jang, S. Hong, G. C. Schatz, and M. A. Ratner, J. Chem. Phys. **115**, 2721 (2001).